

## Au nanoparticle-decorated graphene electrodes for GaN-based optoelectronic devices

Minhyeok Choe,<sup>1</sup> Chu-Young Cho,<sup>1</sup> Jae-Phil Shim,<sup>2</sup> Woojin Park,<sup>1</sup> Sung Kwan Lim,<sup>3</sup> Woong-Ki Hong,<sup>4</sup> Byoung Hun Lee,<sup>1</sup> Dong-Seon Lee,<sup>2</sup> Seong-Ju Park,<sup>1,a)</sup> and Takhee Lee<sup>5,b)</sup>

<sup>1</sup>*School of Materials Science and Engineering, Gwangju Institute of Science and Technology, Gwangju 500-712, Korea*

<sup>2</sup>*School of Information and Communications, Gwangju Institute of Science and Technology, Gwangju 500-712, Korea*

<sup>3</sup>*Department of Nanobio Materials and Electronics, Gwangju Institute of Science and Technology, Gwangju 500-712, Korea*

<sup>4</sup>*Korea Basic Science Institute Jeonju Center, Jeonju 561-756, Korea*

<sup>5</sup>*Department of Physics and Astronomy, Seoul National University, Seoul 151-747, Korea*

(Received 25 April 2012; accepted 2 July 2012; published online 19 July 2012)

We studied GaN-based optoelectronic devices such as light-emitting diodes (LEDs) and solar cells (SCs) with graphene electrodes. A decoration of Au nanoparticles (NPs) on multi-layer graphene films improved the electrical conductivity and modified the work function of the graphene films. The Au NP-decorated graphene film enhanced the current injection and electroluminescence of GaN-based LEDs through low contact resistance and improved the power conversion efficiency of GaN-based SCs through additional light absorption and energy band alignment. Our study will enhance the understanding of the role of Au NP-decorated graphene electrodes for GaN-based optoelectronic device applications. © 2012 American Institute of Physics.

[<http://dx.doi.org/10.1063/1.4737637>]

Graphene has been studied extensively as a promising electrode material in organic and inorganic optoelectronic devices, including light-emitting diodes (LEDs) and solar cells (SCs), due to its transparency, high conductivity, flexibility, low cost, and large-scale manufacturing properties.<sup>1-4</sup> To date, significant efforts have been dedicated to the development of highly conductive graphene films using several strategies, such as sophisticated synthesis processes of graphene, functionalization of the graphene surface, and fabrication of graphene-based nanocomposites.<sup>5-11</sup> For example, the reduced graphene oxide coated with conjugated polymers can improve its contact property through increasing the effectiveness of charge transport.<sup>1,12,13</sup> In particular, the combination of metal nanoparticles (NPs) and graphene is interesting because metal NPs (e.g., Pt, Au, Ag, Al, and Cu) can modify graphene as p- or n-doping. Furthermore, because light scattering is dependent on the size and concentration of the NPs, NPs can be used to alter the optical properties of graphene film. Benayad *et al.*<sup>8</sup> reported that treating graphite oxide with Au NPs enhanced its electrical properties with high transparency and work function controllability for efficient energy band alignment. After decorating graphene oxide films with an Au NP concentration of 20 mM, the sheet resistance had decreased by 53.9% and the work function had increased to 4.9 eV from 4.2 eV. More recently, Chandramohan *et al.*<sup>14</sup> reported a reduction in the specific contact resistance of GaN-based LEDs using multi-layer graphene (MLG) doped with Au NPs and a thin Au metal interlayer. However, additional thin Au interlayer and thermal annealing process may interrupt the Au NP-induced enhancement

of the LED output power. Thus, we focused on the role of Au NP in decorating MLG electrodes using GaN-based optoelectronic devices, such as LEDs and SCs. The light scattering caused by Au NPs reduces the light emission efficiency in the LEDs but enables the SCs to absorb more light energy. Thus, the applied concentration of Au NPs on MLG films ultimately affects the performance of LEDs and SCs.

In this study, we used MLGs that were synthesized with the chemical vapor deposition (CVD) method and treated with two different AuCl<sub>3</sub> solution concentrations (5 mM and 20 mM). Hereafter, the MLGs that were treated with 5 mM and 20 mM AuCl<sub>3</sub> solutions are referred to as “5 mM AuCl<sub>3</sub>-MLG” and “20 mM AuCl<sub>3</sub>-MLG,” respectively. The Au NP-decorated MLGs were applied and investigated as transparent conductive electrodes for the GaN-based LEDs and SCs consisting of multi-quantum-well (MQW) structures.

Graphene films were synthesized with the CVD method. First of all, we deposited polycrystalline Ni films (with a thickness of 300 nm) onto SiO<sub>2</sub>/Si substrates and then transferred these films into a CVD chamber for metal catalytic graphene growth. The Ni-deposited substrates were heated to 900 °C under a 150 sccm flow of 4% H<sub>2</sub> in an Ar gas mixture at ambient pressure. The graphene was then grown after adding 5 sccm of CH<sub>4</sub> gas to the flow for 5 min. After the graphene was grown, the substrate was rapidly cooled to room temperature to prevent the formation of thick multi-layer graphene. Finally, the CVD-grown MLG was released from the Ni layer on the substrate by etching in an aqueous iron chloride (FeCl<sub>3</sub>) solution. Then, the MLGs were immersed into the aqueous AuCl<sub>3</sub> solution with Au NPs at concentrations of 5 and 20 mM. By applying the Au NPs to the MLG, the work function of the MLG could be controlled and its electrical conductivity could be improved. After treatment

<sup>a)</sup>Electronic mail: sjpark@gist.ac.kr.

<sup>b)</sup>Electronic mail: tlee@snu.ac.kr.

with the Au NPs, the MLGs were transferred onto GaN-based LEDs and SCs.

The GaN-based LEDs and SCs were prepared using metalorganic chemical vapor deposition (MOCVD) on a *c*-plane (0001) sapphire substrate. An undoped GaN layer and *n*-GaN layer both with a thickness of 2  $\mu\text{m}$  were grown at 1020  $^{\circ}\text{C}$  on a GaN nucleation layer. The MQWs consisting of periodic undoped InGaN wells and GaN barriers were then grown at 800  $^{\circ}\text{C}$ , followed by the growth of a *p*-GaN layer with a thickness of 200 nm at 980  $^{\circ}\text{C}$ . A *p*-GaN layer was etched through an inductively coupled plasma (ICP) etching process until the *n*-GaN layer was exposed. After the MLG was transferred to the *p*-GaN layer, the MLG in the *n*-contact electrode regions was selectively removed by photolithography and reactive ion etching methods. Finally, an *n*-contact electrode (Cr/Au) was deposited on the *n*-GaN layer, and the photoresist was removed. The MLG acted as a *p*-contact transparent conductive electrode.

We investigated the properties of Au NP-decorated MLG electrodes using various tools; the results of this investigation are summarized in Fig. 1. To verify the energy levels of the Au NP-decorated MLG films, UV photoelectron spectroscopy (UPS) measurements (Fig. 1(a)) were performed using the He I photon line of a He discharge lamp under ultra-high vacuum conditions. The work function ( $\Phi$ ) can be determined from the secondary electron threshold energy as  $\Phi = h\nu - (E_F - E_{\text{cutoff}})$ , where  $h\nu$  is the photon energy of the excitation light (21.2 eV),  $E_F$  is the Fermi level (21.2 eV), which is calibrated by the Fermi level edge of an evaporated Au film shown on the right plot of Fig. 1(a), and  $E_{\text{cutoff}}$  is the inelastic high-binding-energy cutoff.  $E_{\text{cutoff}}$  is extracted using a linear extrapolation of the high-binding-energy cutoff region of the UPS spectra. From Fig. 1(a), the  $E_{\text{cutoff}}$  of the as-grown MLG films was determined to be  $\sim 4.42$  eV, resulting in a work function of 4.42 eV, which is similar to that reported in our previous studies and other literature.<sup>7,15</sup> The work functions of the 5 mM AuCl<sub>3</sub>-MLG and 20 mM AuCl<sub>3</sub>-MLG were increased to 4.77 eV and 5.12 eV, respectively, indicating that the increase of the work function of

the Au NP-decorated MLG is related to the charge (electron) transfer from the MLG to the Au NPs.<sup>8,16,17</sup>

Raman spectroscopy was used to analyze the synthesized MLG films and to study the doping effects of the charge transfer between dopants and carbon materials, providing evidence of the charge carrier density increase.<sup>18</sup> As shown in Fig. 1(b), the Raman spectra of the graphene film had three major peaks, including the D peak at  $\sim 1350$   $\text{cm}^{-1}$  (Fig. 1(b) left), G peak at  $\sim 1580$   $\text{cm}^{-1}$  (Fig. 1(b) middle), and 2D peak at  $\sim 2700$   $\text{cm}^{-1}$  (Fig. 1(b) right). These peaks were shifted upwards or downwards by the dopants, providing substantial evidence for the increased density of the charge carriers, similar to the previously reported doping effects in carbon nanotubes.<sup>10,19</sup> From the intensity ratio of the G and 2D peaks, the CVD-synthesized MLGs typically have multi-layer-type Raman features (G peak intensity  $>$  2D peak intensity). Furthermore, the D peak increased slightly after incorporating the Au NPs onto the MLG films, indicating the formation of disorder or defects, as induced by the Au NPs. Furthermore, the G and 2D peaks of the Au NP-decorated MLG films shifted upwards when compared with those of the as-grown MLG samples due to changes in the charge carrier density. Here, electrons were transferred from the graphene to the Au NPs, indicating a hole-doping effect in the graphene.

To apply the Au NP-decorated MLG films as transparent conductive electrodes for optoelectronics, we investigated the optical transmittances and sheet resistances of three types of MLGs. As expected, the MLG with high-density Au NPs yielded a lower transmittance. The optical transmittances shown in Fig. 1(c) were approximately 89, 85, and 78% at a 400 nm wavelength for the as-grown MLG, 5 mM AuCl<sub>3</sub>-MLG, and 20 mM AuCl<sub>3</sub>-MLG, respectively.

To confirm the carrier density and electrical conductivity of the MLGs, we performed the van der Pauw four-probe method using a Hall measurement.<sup>20</sup> Figure 1(d) shows the sheet resistances and hole-carrier densities of the three types of MLGs. An inversely proportion relationship between the sheet resistance and hole-carrier density as a function of the Au NP concentration was observed. The sheet resistances and hole-carrier densities were  $1000 \pm 98$   $\Omega/\square$  and  $(9.6 \pm 2.9) \times 10^{12}/\text{cm}^3$  for the as-grown MLG,  $203 \pm 37$   $\Omega/\square$  and  $(9.5 \pm 4.0) \times 10^{13}/\text{cm}^3$  for the 5 mM AuCl<sub>3</sub>-MLG, and  $105 \pm 7$   $\Omega/\square$  and  $(2.4 \pm 0.4) \times 10^{14}/\text{cm}^3$  for the 20 mM AuCl<sub>3</sub>-MLG, respectively. Figure 1(d) was obtained after calculating the statistical averages and standard deviations of 9–12 different MLGs at each Au NP concentration. The transmittance and sheet resistance results indicate that high-density Au NPs not only induce a lower resistance but also induce a lower level of transparency in the MLG films. In addition, by using transmission electron microscope (TEM), we investigated the structural properties of MLG films and found they had multi-layer features ( $\sim 9$  layers) with an interlayer distance of  $3.9 \pm 0.1$   $\text{\AA}$  (see the supplementary materials).<sup>28</sup>

Regarding the analyses of the Au NP-decorated MLG, we fabricated the GaN-based LEDs and SCs with Au NP-decorated MLG instead of indium tin oxide (ITO) and investigated the role of Au NPs on MLG electrodes for both of the optoelectronic devices. Figure 2(a) shows the schematic illustration of the GaN-based LED with an MQW configuration. Detailed information on the device fabrication is

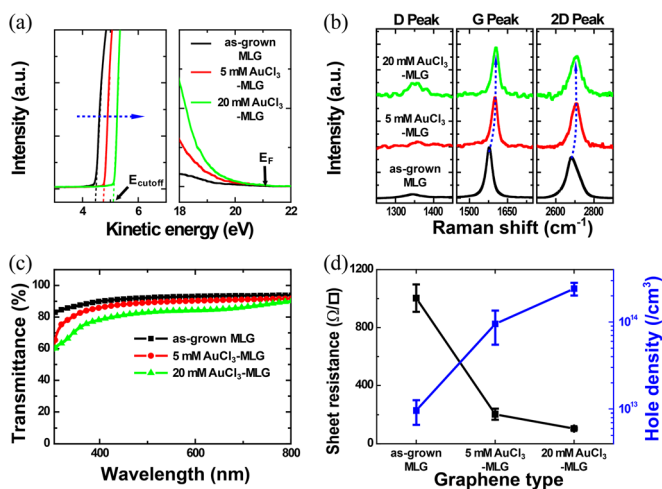


FIG. 1. (a) UPS spectra of the MLG films (as-grown MLG, 5 mM AuCl<sub>3</sub>-MLG, and 20 mM AuCl<sub>3</sub>-MLG) with different Au NP concentrations. (b) The Raman spectra and (c) transmittance characteristics of the MLGs (as-grown MLG, 5 mM AuCl<sub>3</sub>-MLG, and 20 mM AuCl<sub>3</sub>-MLG). (d) The sheet resistance and hole-carrier density measured using the Hall method.

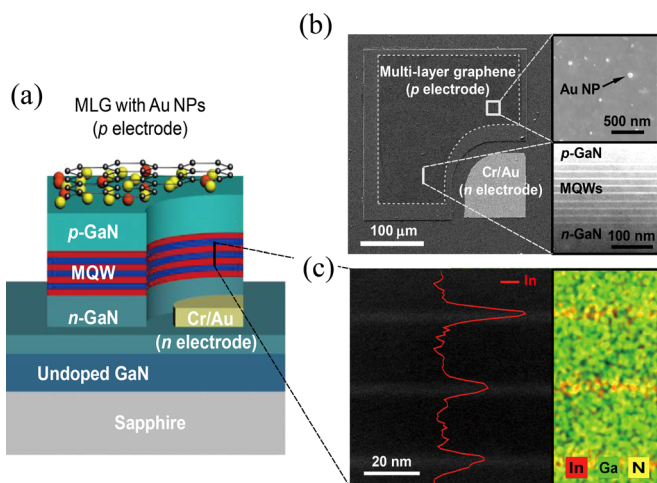


FIG. 2. (a) Schematic illustration of MLG-electrode GaN-based LED device. (b) A plan-view SEM image of a GaN-based LED device. The insets show an SEM image of the MLG with Au NPs (top) and a TEM image of the multiple quantum wells (bottom). (c) A magnified TEM image and the EDX mapping of the MQWs.

provided in the supplementary materials.<sup>28</sup> Figure 2(b) shows the plan-view scanning electron microscope (SEM) images (right upper inset in Fig. 2(b)) and a cross-section TEM image (right lower inset in Fig. 2(b)) of a GaN-based LED with 20 mM AuCl<sub>3</sub>-MLG. The number density of the Au NPs was found to be  $\sim 1.1 \times 10^9/\text{cm}^2$  and the surface area coverage was  $\sim 3.5\%$  for the 20 mM AuCl<sub>3</sub>-MLG, estimated from SEM images (see the supplemental materials<sup>28</sup>). The insets in Fig. 2(b) clearly show the Au NPs formed on MLG and the periodic MQWs. Furthermore, TEM energy-dispersive x-ray spectroscopy (EDX) mapping of the GaN-based LED was performed to confirm the elemental composition of the MQWs (Fig. 2(c)). The undoped InGaN wells were well-separated and periodically constructed for the efficient recombination of the electron-hole pairs.

Figure 3(a) shows the  $I$ - $V$  characteristics of the resulting MLG-electrode GaN-based LEDs. The forward voltages measured at 0.4 mA were 4.73, 3.94, and 3.86 V for the GaN-based LEDs with the as-grown MLG, 5 mM AuCl<sub>3</sub>-MLG, and 20 mM AuCl<sub>3</sub>-MLG, respectively. The lower forward voltage can be attributed to the low resistive contact and small work function difference between the 20 mM AuCl<sub>3</sub>-MLG and  $p$ -GaN, forming a high current injection in the MQWs.<sup>21,22</sup> These results can be explained with the electroluminescence (EL) spectra at the 400 nm wavelength in the near-UV range as a function of the injection currents, which vary from 50  $\mu\text{A}$  to 500  $\mu\text{A}$  in increments of 50  $\mu\text{A}$ , as shown in Fig. 3(b). The EL intensity increased with the injection current, and the EL peak position did not shift noticeably, indicating that the MLG acted as a  $p$ -contact electrode in the GaN-based LEDs in a suitable manner. However, the injection current of the MLG-electrode GaN-based LEDs was less than that of the ITO-electrode GaN-based LEDs.<sup>23,24</sup> The EL intensity of the GaN-based LEDs with the 5 mM AuCl<sub>3</sub>-MLG at 500  $\mu\text{A}$  increased by 93.8% and 28.7% when compared to that of the GaN-based LEDs with the as-grown MLG and 20 mM AuCl<sub>3</sub>-MLG, respectively (Fig. 3(c)). Although the 20 mM AuCl<sub>3</sub>-MLG showed higher electrical conductivity than the 5 mM AuCl<sub>3</sub>-MLG, the GaN-

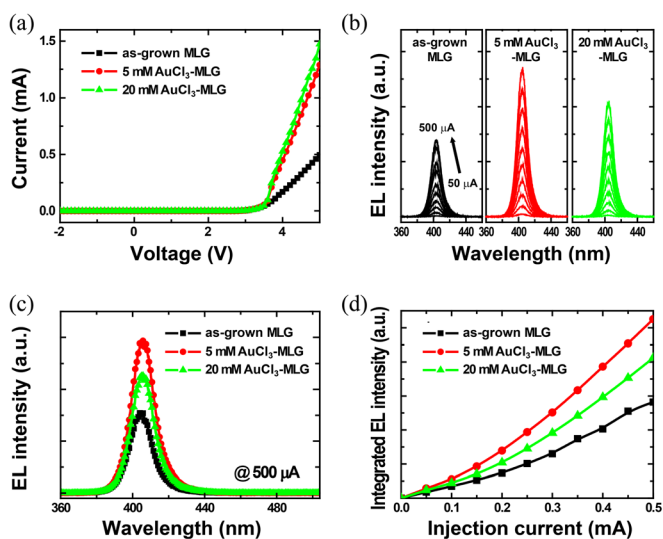


FIG. 3. (a)  $I$ - $V$  curves of the GaN-based LEDs with as-grown MLG, 5 mM AuCl<sub>3</sub>-MLG, and 20 mM AuCl<sub>3</sub>-MLG. (b) The EL intensity of the MLG-electrode GaN-based LEDs as a function of the injection currents. (c) The EL intensity of the MLG-electrode GaN-based LEDs measured at 500  $\mu\text{A}$ . (d) The integrated EL intensity of the MLG-electrode GaN-based LEDs as a function of the injection current.

based LEDs with the 20 mM AuCl<sub>3</sub>-MLG exhibited a lower EL intensity. This is due to the difference in surface coverage of Au NPs which is 0.29% and 3.47% for 5 mM AuCl<sub>3</sub>-MLG and for 20 mM AuCl<sub>3</sub>-MLG, respectively, leading to reduce the transmittance of Au NP-decorated MLGs as shown in Fig. 1(c). To more distinctly compare the light emission, we integrated the EL intensity as a function of the injection current, as shown in Fig. 3(d). The integrated EL intensity of the GaN-based LEDs with 5 mM AuCl<sub>3</sub>-MLG was 27.4% higher than that of the GaN-based LEDs with 20 mM AuCl<sub>3</sub>-MLG when measured at 500  $\mu\text{A}$ . The decrease in the integrated EL intensity can be attributed to the poor transmittance and light scattering resulting from the high-density Au NPs. By optimizing the concentration of the Au NPs for electrical conductivity and transparency, the current injection and light emission efficiency of the MLG-electrode GaN-based LEDs may be further enhanced.

The light scattering effect by high-density Au NPs in the MLG could reduce the light emission efficiency of GaN-based LEDs; however, the light harvesting efficiency of GaN-based SCs could also be enhanced. Zhu *et al.*<sup>25</sup> reported that nanotube-based dye-sensitized SCs had higher light harvesting efficiencies due to light scattering effects. We also investigated the transparent, conductive, MLG-electrode GaN-based SCs. The structure and composition of the MQWs and the fabrication process of the GaN-based SCs were identical to those of the GaN-based LEDs (Fig. 2(a)). Figure 4(a) shows the current density-voltage ( $J$ - $V$ ) characteristics of the resulting MLG-electrode GaN-based SCs under AM 1.5 G irradiation by a solar simulator with an irradiation intensity of 100 mW/cm<sup>2</sup>. The best performance was achieved using the GaN-based SCs with the 20 mM AuCl<sub>3</sub>-MLG. Specifically, the optimal parameters obtained for the GaN-based SCs with the 20 mM AuCl<sub>3</sub>-MLG were a short-circuit current ( $J_{\text{SC}}$ ) of 0.67 mA/cm<sup>2</sup>, an open-circuit voltage ( $V_{\text{OC}}$ ) of 2.25 V, and a fill factor (FF) of 0.77. These values yielded a peak-to-correlation energy (PCE),  $\eta_e = J_{\text{SC}} V_{\text{OC}} \text{FF} / P_{\text{inc}}$

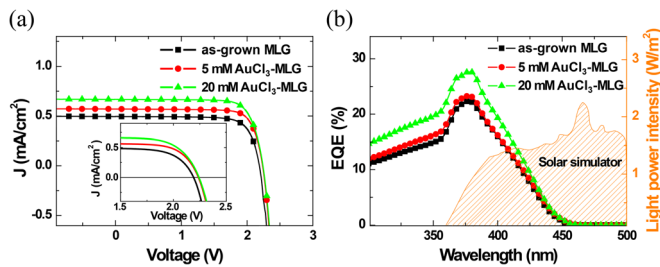


FIG. 4. (a) J-V curves of the GaN-based SCs with as-grown MLG, 5 mM AuCl<sub>3</sub>-MLG, and 20 mM AuCl<sub>3</sub>-MLG under AM 1.5G irradiation conditions. The inset shows the zoomed-in J-V curve near the current density of 0 mA/cm<sup>2</sup>. (b) EQE of the fabricated MLG-electrode, GaN-based SCs. The shaded area denotes the solar spectrum.

(here,  $P_{\text{inc}}$  is the intensity of the incident light), of 1.2%. The PCE value (1.2%) of the GaN-based SCs with the 20 mM AuCl<sub>3</sub>-MLG was larger than that of the GaN-based SCs with as-grown MLG (0.9%) due to the increases in  $V_{\text{OC}}$  and  $J_{\text{SC}}$ . Furthermore, the  $J_{\text{SC}}$  value (0.67 mA/cm<sup>2</sup>) of the GaN-based SCs with the 20 mM AuCl<sub>3</sub>-MLG was greater than that of the GaN-based SCs with the as-grown MLG (0.51 mA/cm<sup>2</sup>). The increase in  $J_{\text{SC}}$  can be explained in terms of the improved electrical conductivity and light absorption induced by the Au NPs in the 20 mM AuCl<sub>3</sub>-MLG. Furthermore,  $V_{\text{OC}}$  increased slightly due to the lower energy level offset between the 20 mM AuCl<sub>3</sub>-MLG and *p*-GaN layer compared to that between the as-grown MLG and *p*-GaN layer. As shown in Fig. 1(a), the work function of the 20 mM AuCl<sub>3</sub>-MLG shifted from 4.42 eV to 5.12 eV, indicating that the 20 mM AuCl<sub>3</sub>-MLG with a high work function facilitates a better band energy alignment for the transport of dissociated holes to the *p*-contact electrode.<sup>26,27</sup> The performance parameters for the MLG-electrode GaN-based SCs are statistically summarized in Table S1 in the supplementary materials.<sup>28</sup>

Figure 4(b) displays the external quantum efficiency (EQE) as a function of the excitation wavelength for the MLG-electrode GaN-based SCs. The three major factors for improving the EQE in GaN-based SCs are the following: (1) the light absorption should be enhanced with a conductive transparent *p*-contact electrode as a current spreading layer; (2) the thickness and period optimization of the MQWs should maximize the photo-generated electron-hole pairs and minimize other detrimental effects due to the high In content in InGaN alloys; and (3) the InGaN alloys should have a good crystalline quality, which is a remaining issue in this research field. In this study, by applying Au NPs on MLG, light scattering occurred and increased the EQEs of GaN-based SCs. The GaN-based SCs exhibited a maximum EQE of 28% at 380 nm and 5% at 435 nm, i.e., light absorption occurred within a range of 350 to 450 nm. Despite the lower transmittance of the 20 mM AuCl<sub>3</sub>-MLG, the EQE of the GaN-based SCs with the 20 mM AuCl<sub>3</sub>-MLG was larger than that of the GaN-based SCs with the as-grown MLG due to the efficient light absorption resulting from the light scattering by Au NPs.

In summary, we investigated Au NP-decorated MLG electrodes for GaN-based LEDs and SCs. The Au NPs increased the conductivity and light scattering of the MLG films and changed their work function. These effects of the Au NPs on the MLG films improved the current injection and electroluminescence of the LEDs and the power conver-

sion efficiency of the SCs. The light scattering of the high-density Au NPs on the MLG films increased the light-harvesting efficiency of the GaN-based SCs but reduced the light emission efficiency of the GaN-based LEDs. This study provides useful insights in terms of the role of Au NP-decorated graphene electrodes for GaN-based and other types of optoelectronic device applications.

This work was supported by the Inter-ER Cooperation Projects (Grant No. R0000499) from the Ministry of Knowledge Economy (MKE), the National Research Laboratory, a Korean National Core Research Center grant from the Korean Ministry of Education, Science, and Technology, the Korea Institute of Science and Technology (KIST) Institutional Program, the National Research Foundation of Korea (Grant No. 20120002256), and the Research Settlement Fund for the new faculty of Seoul National University.

- <sup>1</sup>X. Wan, G. Long, L. Huang, and Y. Chen, *Adv. Mater.* **23**, 5342 (2011).
- <sup>2</sup>C. Biswas and Y. H. Lee, *Adv. Funct. Mater.* **21**, 3806 (2011).
- <sup>3</sup>Y. Gao, H.-L. Yip, K.-S. Chen, K. M. O'Malley, O. Acton, Y. Sun, G. Ting, H. Chen, and A. K. Y. Jen, *Adv. Mater.* **23**, 1903 (2011).
- <sup>4</sup>A. Kumar and C. Zhou, *ACS Nano* **4**, 11 (2010).
- <sup>5</sup>X. Li, W. Cai, J. An, S. Kim, J. Nah, D. Yang, R. Piner, A. Velamakanni, I. Jung, E. Tutuc, S. K. Banerjee, L. Colombo, and R. S. Ruoff, *Science* **324**, 1312 (2009).
- <sup>6</sup>K. S. Kim, Y. Zhao, H. Jang, S. Y. Lee, J. M. Kim, K. S. Kim, J.-H. Ahn, P. Kim, J.-Y. Choi, and B. H. Hong, *Nature (London)* **457**, 706 (2009).
- <sup>7</sup>M. Choe, B. H. Lee, G. Jo, J. Park, W. Park, S. Lee, W.-K. Hong, M.-J. Seong, Y. H. Kahng, K. Lee, and T. Lee, *Org. Electron.* **11**, 1864 (2010).
- <sup>8</sup>A. Benayad, H.-J. Shin, H. K. Park, S.-M. Yoon, K. K. Kim, M. H. Jin, H.-K. Jeong, J. C. Lee, J.-Y. Choi, and Y. H. Lee, *Chem. Phys. Lett.* **475**, 91 (2009).
- <sup>9</sup>G. Giovannetti, P. A. Khomyakov, G. Brocks, V. M. Karpan, J. van den Brink, and P. J. Kelly, *Phys. Rev. Lett.* **101**, 026803 (2008).
- <sup>10</sup>P. V. Dudin, P. R. Unwin, and J. V. Macpherson, *J. Phys. Chem. C* **114**, 13241 (2010).
- <sup>11</sup>Y. Shi, K. K. Kim, A. Reina, M. Hofmann, L.-J. Li, and J. Kong, *ACS Nano* **4**, 2689 (2010).
- <sup>12</sup>H. Bai, C. Li, and G. Shi, *Adv. Mater.* **23**, 1089 (2011).
- <sup>13</sup>Z. Liu, L. Liu, H. Li, Q. Dong, S. Yao, A. B. Kidd IV, X. Zhang, J. Li, and W. Tian, *Sol. Energy Mater. Sol. Cells* **97**, 28 (2012).
- <sup>14</sup>S. Chandramohan, J. H. Kang, Y. S. Katharria, N. Han, Y. S. Beak, K. B. Ko, J. B. Park, H. K. Kim, E.-K. Suh, and C.-H. Hong, *Appl. Phys. Lett.* **100**, 023502 (2012).
- <sup>15</sup>J. Wu, H. A. Becerril, Z. Bao, Z. Liu, Y. Chen, and P. Peumans, *Appl. Phys. Lett.* **92**, 263302 (2008).
- <sup>16</sup>S. Kazaoui, N. Minami, R. Jacquemin, H. Kataura, and Y. Achiba, *Phys. Rev. B* **60**, 13339 (1999).
- <sup>17</sup>B.-S. Kong, D.-H. Jung, S.-K. Oh, C.-S. Han, and H.-T. Jung, *J. Phys. Chem. C* **111**, 8377 (2007).
- <sup>18</sup>A. M. Rao, P. C. Eklund, S. Bandow, A. Thess, and R. E. Smalley, *Nature (London)* **388**, 257 (1997).
- <sup>19</sup>V. Georgakilas, D. Gournis, V. Tzitzios, L. Pasquato, D. M. Guldi, and M. Prato, *J. Mater. Chem.* **17**, 2679 (2007).
- <sup>20</sup>L. J. van der Pauw, *Philips Res. Rep.* **13**, 1 (1958).
- <sup>21</sup>T.-Y. Park, Y.-S. Choi, J.-W. Kang, J.-H. Jeong, S.-J. Park, D. M. Jeon, J. W. Kim, and Y. C. Kim, *Appl. Phys. Lett.* **96**, 051124 (2010).
- <sup>22</sup>J. Dai, Y. Ji, C. X. Xu, X. W. Sun, K. S. Leck, and Z. G. Ju, *Appl. Phys. Lett.* **99**, 063112 (2011).
- <sup>23</sup>J. Gunho, C. Minhyeok, C. Chu-Young, K. Jin Ho, P. Woojin, L. Sangchul, H. Woong-Ki, K. Tae-Wook, P. Seong-Ju, H. Byung Hee, K. Yung Ho, and L. Takhee, *Nanotechnology* **21**, 175201 (2010).
- <sup>24</sup>J. M. Lee, J. W. Choung, J. Yi, D. H. Lee, M. Samal, D. K. Yi, C.-H. Lee, G.-C. Yi, U. Paik, J. A. Rogers, and W. I. Park, *Nano Lett.* **10**, 2783 (2010).
- <sup>25</sup>K. Zhu, N. R. Neale, A. Miedaner, and A. J. Frank, *Nano Lett.* **7**, 69 (2006).
- <sup>26</sup>C.-Y. Kuo, M.-S. Su, Y.-C. Hsu, H.-N. Lin, and K.-H. Wei, *Adv. Funct. Mater.* **20**, 3555 (2010).
- <sup>27</sup>C. J. Brabec, A. Cravino, D. Meissner, N. S. Sariciftci, T. Fromherz, M. T. Rispens, L. Sanchez, and J. C. Hummelen, *Adv. Funct. Mater.* **11**, 374 (2001).
- <sup>28</sup>See supplementary material at <http://dx.doi.org/10.1063/1.4737637> for cross-section TEM image.